RSC Advances

This is an *Accepted Manuscript*, which has been through the Royal Society of Chemistry peer review process and has been accepted for publication.

Accepted Manuscripts are published online shortly after acceptance, before technical editing, formatting and proof reading. Using this free service, authors can make their results available to the community, in citable form, before we publish the edited article. This *Accepted Manuscript* will be replaced by the edited, formatted and paginated article as soon as this is available.

You can find more information about *Accepted Manuscripts* in the Information for Authors.

Please note that technical editing may introduce minor changes to the text and/or graphics, which may alter content. The journal's standard Terms & Conditions and the Ethical guidelines still apply. In no event shall the Royal Society of Chemistry be held responsible for any errors or omissions in this *Accepted Manuscript* or any consequences arising from the use of any information it contains.

ROYAL SOCIETY OF CHEMISTRY

www.rsc.org/advances

Energetics of Proton Transfer in Alkali Carbonates: a First Principles Calculation

Xueling Lei [a, b], Changyong Qin [c] and Kevin Huang [b,*]

[a] Department of Physics, Jiangxi Normal University, Nanchang, Jiangxi 330022, China

[b] Department of Mechanical Engineering, University of South Carolina, Columbia, SC 29208, USA

[c] Department of Biology, Chemistry and Environmental Health Science, Benedict College, Columbia, South Carolina 29204, USA

Abstract

Recent development of dual-phase ceramic-carbonate composite electrolytes for intermediate-temperature solid oxide fuel cells (SOFCs) has prompted a pressing question on whether H^+ can transfer in molten carbonates and play a role in the enhanced ionic conductivity and improved SOFC performance. In the present study, we use a first principles approach to examining the energetics of H^+-transfer in CO_3^{2-}, Li_2CO_3 crystal and $(Li_2CO_3)_8$ cluster. The results indicate that H^+-transfer in solid carbonates is difficult, but very facile in a $(Li_2CO_3)_8$ cluster, a surrogate of molten carbonates.

Keywords: ionic conductivity; proton transfer; carbonates; energetics, first principles

* Corresponding author: Kevin Huang, huang46@cec.sc.edu.

RSC Advances Accepted Manuscript

1. Introduction

A focus of the current effort to commercialize solid oxide fuel cell (SOFC) technology is to lower the operating temperature to below 600^{o}C where high reliability and low cost can be achieved. The major barrier to the realization of reduced temperature SOFCs is the lack of high-conductivity electrolyte and high-activity catalytic cathodes. A noticeable development of the former in recent years is the use of dual-phase composite comprising of a solid ionic conductor and carbonate as the intermediate-temperature (IT) electrolytes [1-10]. Testing of these composite electrolytes in a SOFC has yielded high power density in the IT range [7-9]. To understand the high performance, a number of ionic conduction mechanisms have been proposed. For example, Zhu *et al* [3-5] proposed a binary O^{2-}/H^{+} conduction mechanism to explain the enhanced conductivity for a ceria-carbonate electrolyte. Similarly, Li *et al* proposed a ternary $O^{2-}/H^{+}/CO_3^{2-}$ conduction mechanism to account for the enhanced conductivity and SOFC performance for a samarium-doped cerium oxide (SDC)/Li-Na-K carbonate composite [8-9]. Recently, we have also formulated several ionic conduction mechanisms to understand the enhanced ionic conductivity in the presence of water vapor in a $BaZr_{0.8}Y_{0.2}O_{3-\delta}$ (BZY) and a Li-K carbonate composite electrolyte [10].

A close examination of the aforementioned ionic conduction mechanisms suggests that proton conduction in molten carbonates may play an important role in the enhanced ionic conductivity and subsequently SOFC performance. However, how protons transfer in molten carbonates remains mechanistically ambiguous at this point. To the best of our knowledge, there have been neither theoretical nor experimental investigations on proton transfer in molten carbonates in the open literature other than proton transfer in an aqueous $KHCO_3$

RSC Advances Accepted Manuscript

system [11-12].

In this study, we use first principles approach to calculating the energetics of proton transfer in three entities: CO_3^{2-}, Li_2CO_3 crystal and $(Li_2CO_3)_8$ cluster to provide a theoretical ground for the understanding of enhanced ionic conductivity and improved SOFC performance observed in the experiments. A $(Li_2CO_3)_8$ cluster was employed to represent the state of an alkali molten carbonate.

2. Computational methods

2.1 Calculations for $(CO_3)^{2-}$ and $(CO_3H)^-$ ions, and periodic structures

All calculations for $(CO_3)^{2-}$ and $(CO_3H)^-$ ions, and periodic structures were performed using the Vienna Ab-Initio Simulation Package (VASP), version 5.3 [13-14]. The projector-augmented wave (PAW) method was used for calculating core and valence electron interactions [15-16], while the Perdew–Burke–Ernzerhof (PBE) form of the generalized gradient approximation (GGA) was used to describe the exchange–correlation interaction [17]. The cut-off energy of the plane wave basis representing valence electrons was set to 500 eV. The self-consistent field cycle convergence tolerance was set to 10^{-4} eV and the Hellmann–Feynman force on each atom was minimized to less than 0.02 eV $Å^{-1}$. The proton transport properties were modeled using a 3×2×2 k-point grid for a 96-atom supercell. The climbing image-nudged elastic band (CI-NEB) method [18] was employed to find the minimum energy paths and transition states for proton transfer. A vacuum layer of 15 Å has been applied for $(CO_3)^{2-}$ and $(CO_3H)^-$ ions.

2.2 Calculations for $(Li_2CO_3)_8$ and $[(Li_2CO_3)_8H]^+$ clusters

RSC Advances Accepted Manuscript

For cluster systems, combining SCAN with TS functions in Gaussian suite of quantum program can be easily used to search the transition state, while the IRC function can help judge the reaction direction. To illustrate that Gaussian is a valid method for calculating transition state and reaction direction, we also performed test calculations by VASP 5.3 [13-14] and Gaussian 09 [19], respectively. The structures of $(CO_3)^{2-}$ and $(CO_3H)^-$ ions were optimized and the energy barrier of proton transfer in intra-carbonate ion $(CO_3)^{2-}$ were calculated. It was found that the deviation between the two methods were generally small: bond length: ~1% for bond length, 0.1-1.0% for bond angle, 14-16% for energy barrier. It is, therefore, reasonable to believe that Gaussian 09 can produce representative energy barrier of proton transfer in the $(Li_2CO_3)_8$ cluster.

All calculations for $(Li_2CO_3)_8$ and $[(Li_2CO_3)_8H]^+$ clusters were performed by Gaussian 09 suite of quantum programs, including the geometry optimization, transition state search and intrinsic reaction coordinate (IRC) calculations. The geometries were optimized by using the generalized gradient approximation (GGA) based hybrid functional of B3LYP [20-21] in combination with the full-electron basis set with polarization functions of 6-31G (d) [22-24] to obtain accurate results. B3LYP has been proven to be reliable in treating electronic exchange and correlation over a wide range of molecular systems. The vibrational frequencies of each cluster were calculated at the same computational level as the geometry optimization, ensuring that the structures are located at a true minimum on the potential energy surface and the transition state is a first-order saddle point on the potential energy surface. All resulting energies contained the zero-point energy (ZPE) corrections. In addition, the interactions between proton and carbonate ions are orbital overlap and electrostatic interactions.

RSC Advances Accepted Manuscript

Therefore, the dispersive interactions can be ignored in our calculations.

3. Results and discussion

3.1 Proton migration in CO_3^{2-} in gas phase

Before examining proton migration in gas-phase $(CO_3)^{2-}$, we first optimized the structures of $(CO_3)^{2-}$ and $(CO_3H)^-$ ions. The bond distances and angles are shown in Fig. 1(a)-(b). Both structures feature a planar geometry. In $(CO_3)^{2-}$ of D_{3h} symmetry, all the calculated C-O bond lengths are 1.295 Å, which reasonably agree well with the literature results of 1.306 Å [25] and 1.309 Å [26]. All the bond angles of O-C-O are 120°. Addition of proton to the $(CO_3)^{2-}$ forms planar $(CO_3H)^-$ of C_s symmetry, where the bond angle of H-O-C is 101.2° and the bond length of O-H is 0.976 Å.

Fig. 2(a)-(b) shows the H^+-migration in a gas-phase $(CO_3)^{2-}$. Here, we select two representative motions: planar transfer between two oxygen atoms and rotation along one oxygen atom. The first motion is shown in Fig. 2(a), where H^+ (in white color) migrates from O1 to O2. During this transfer, the bond between O1 and H^+ is first broken, followed by H^+ moving toward the mirror position between O1 and O2, namely the transition state. The bond between O2 and H^+ is then reformed, completing the H^+-transfer. We found that the energy barrier for H^+-transfer between O1 and O2 was 0.89 eV.

Unlike the H^+-migration through intra-oxygen shown in Fig. 2(a), Fig. 2(b) shows H^+-transfer through H^+-rotation along O1 atom. Likewise, a transition state was searched by NEB method. As shown in Fig. 2(b), H^+ on the left side of O1 rotates along O1, passing through the transition state above the O1 atom, reaching the right side of O1. During this

RSC Advances Accepted Manuscript

process, the bond between O1 and H^+ remains, and the transfer only needs to overcome an energy barrier of 0.40 eV. Clearly, the rotation mechanism is energetically more favorable than the intra-oxygen transfer mechanism for H^+-migration in $(CO_3)^{2-}$. Such a low energy barrier also implies that lower thermal energy (or lower temperature) is needed to drive H^+-migration in $(CO_3)^{2-}$.

3.2 Proton migration in Li_2CO_3 crystal

We are also interested in H^+-migration in a crystalline carbonate, the material of which under this study is lithium carbonate (Li_2CO_3) having a monoclinic structure and *C*2/*c* space group. The optimized crystal structure of a Li_2CO_3 is shown in Fig. 3. There are four formula units in a primitive cell as shown in Fig. 3(a). The calculated lattice parameters are a = 8.397 Å, b = 5.019 Å, c = 6.311 Å; α = 89.99 °, β = 114.63 °, γ = 90.00 °, which agree reasonably well with the experimental values: a = 8.39 Å, b = 5.00 Å, c = 6.21 Å; α = 90.00 °, β = 114.5 °, γ = 90.00 ° [27]. To simulate the H^+-transfer in Li_2CO_3, a supercell containing a 1×2×2 cell is constructed and shown in Fig.3 (b).

From analysis of the symmetry of the Li_2CO_3 crystal structure, four representative migration pathways of H^+-transfer along a, b, c, and ca directions are considered, as shown in Fig. 4 (a), (b), (c), and (d), respectively. In Fig. 4, [100], [010] [001], and [101] represent the directions of H^+-transfer along a, b, c, and ca, respectively. On the other hand, $[\bar{1}00]$, $[0\bar{1}0]$, $[00\bar{1}]$ and $[\bar{1}0\bar{1}]$ represent the H^+-transfer along -a, -b, -c, and -ca directions, respectively. Generally, there are three possible motions of H^+ in Li_2CO_3: (1) rotation – the proton rotates around one oxygen ion while still remaining bonded to the oxygen ion; (2)

RSC Advances Accepted Manuscript

intra-carbonate ion transfer – the proton moves from one oxygen ion to another oxygen ion of the same carbonate ion; (3) inter-carbonate ion transfer – the proton moves from one oxygen ion to another oxygen ion of a different carbonate ion. For convenience, we used small case letter a, b, c … to denote the possible proton locations and capital T and R to represent proton transfer between oxygen and rotation along one oxygen. For example, T_{ab} refers to proton transferring between two O atoms from a to b, and R_{bc} refers to proton rotation along one O from b to c. The energy barriers for H^+-migration involved in these pathways are summarized in Table 1-4.

Fig. 4(a) shows the H^+-transfer pathway via $T_{ab} \rightarrow T_{bc} \rightarrow R_{cd} \rightarrow T_{da}$ along the [100] direction. From Table 1, the T_{ab} and T_{ba} pathways involve H^+-transfer between two O of one $(CO_3)^{2-}$ and present a higher migration energy barrier of 0.85 eV. By contrast, R_{cd} and R_{dc} pathways represent H^+-transfer through rotation along one O of $(CO_3)^{2-}$ and yield a lower migration energy barrier of 0.58 eV. These findings agree well with the results of H^+-migration in a $(CO_3)^{2-}$ at gas phase (see section 3.1).

The H^+-transfer along the [010] direction only includes two steps: inter-carbonate ion transfer (T_{ef}) and intra-carbonate ion transfer (T_{fg}). The former needs to overcome the energy barrier of 0.37 eV, and the latter needs to overcome a higher barrier of 1.10 eV. On the contrary, the highest energy barrier along $[0\bar{1}0]$ direction is found to be 0.83 eV in the intra-carbonate ion transfer (T_{gf}) process.

Similarly, the pathway along the [001] direction can undergo by the following sequence: $T_{hi} \rightarrow R_{ij} \rightarrow T_{jh}$. The highest migration barriers are found to be 0.34 and 0.48 eV for [001]

RSC Advances Accepted Manuscript

and $[00\bar{1}]$ directions, respectively.

Furthermore, Fig. 4(d) shows the H^+-transfer pathway via $R_{kl} \rightarrow T_{lm} \rightarrow R_{mn} \rightarrow T_{no} \rightarrow R_{op} \rightarrow T_{pk}$ along $[101]$ direction. From Table 4, we can see that the R_{kl} yields the highest migration energy barrier of 1.13 eV along $[101]$, followed by R_{lk} of 0.91 eV along $[\bar{1}0\bar{1}]$, T_{lm} and T_{ml} of 0.84 eV along $[101]$ and $[\bar{1}0\bar{1}]$ direction, respectively.

Comparison of the above energetics suggests that the H^+-transfers in a crystalline Li_2CO_3 along $[001]$ and $[00\bar{1}]$ directions is more favorable than other directions. The reason for the favorable H^+-migration stems from the relative crystallographic positions of $(CO_3)^{2-}$ to c-axis. As is shown in Fig. 3, the $(CO_3)^{2-}$ plane is perpendicular to c-axis along the $[001]$ and $[00\bar{1}]$, making the rotational H^+-transfer geometrically easier. On the other hand, when the proton transfers between inter-carbonate ions, the carbonate ions also adjust their position accordingly, decreasing the energy barrier of H^+-transfer. However, it is almost parallel to a-axis, b-axis and ac direction along the $[100]$, $[010]$, $[101]$, $[\bar{1}00]$, $[0\bar{1}0]$, and $[\bar{1}0\bar{1}]$ directions, such as T_{ab}, T_{fg} and T_{lm}, which requires H^+ to transfer between two O in a $(CO_3)^{2-}$. As aforementioned, H^+-transfer via intra-oxygen mechanism has a higher energy barrier.

3.3 Proton migration in $(Li_2CO_3)_8$ cluster

Since the experiments that showed an enhanced ionic conductivity and improved SOFC performance involved molten carbonates, we are also interested in H^+-transfer in the molten state of carbonates. Here we used a cluster of $(Li_2CO_3)_8$ to represent a disordered molten carbonate. Fig. 5 shows the structure of cluster $(Li_2CO_3)_8$ and the structural states of beginning, transitioning and ending phases of proton transfer in the $(Li_2CO_3)_8$ cluster

RSC Advances Accepted Manuscript

together with the relative energies. The $(Li_2CO_3)_8$ clusters at the b3lyp/6-31g (d) level were first optimized. As illustrated in Fig. 5 (a), each Li^+ is bonded to three carbonate O^{2-}, while each carbonate O^{2-} is connected to two Li^+. Such a coordination is the same as those in the crystal structures of Li_2CO_3. In addition, the average bond length between Li^+ and O^{2-} (d_{Li-O}) in $(Li_2CO_3)_8$ is calculated to be 1.948 Å, which agrees well with experimental values of 1.960 Å [28]. Our recent *ab initio* molecular dynamics (AIMD) study confirms that the volume expansion of Li_2CO_3 is only 3% at the temperature of 1300 K (calculated melting point ~1000 K), implying that the Li-O bond length would not change significantly in the molten lithium carbonate. All evidences above suggest that using $(Li_2CO_3)_8$ to describe the structure of molten carbonates be reasonable.

Next, the stable structure of $[(Li_2CO_3)_8H]^+$ cluster is also obtained at the b3lyp/6-31g (d) level. To examine how the proton migration takes place on the atomic scale, we first locate a transition state (Fig. 5 (c)) through the SCAN and TS functions implanted in Gaussian 09 package, followed by IRC calculation. Then, we optimized the two end point structures of IRC to obtain the accurate structures of reaction and product, as shown in Fig. 5 (b) and (d). As seen from Fig. 5, the H^+ bonds with Oa as the reactant and bonds with Ob as the product. The IRC calculations specify that the H^+ first departs from Oa to the middle point between Oa and Ob, reaching the TS. During this process, the bond between H^+ and Oa is enlarged from 1.018 Å to 1.237 Å with a very small energy barrier of 0.08 eV. Then the H^+ separates from Oa and continues to move towards Ob. Meanwhile, the bond length of H^+-Oa increases from 1.237 Å to 1.399 Å, whereas the bond length of H^+-Ob reduces from 1.170 Å to 1.069 Å, thus completing a single H^+-transfer process. In addition, the low TS-to-product energy

RSC Advances Accepted Manuscript

barrier also suggests that the transition from product to reactant is a reversible process, which further implies that continuous H^+-transfer in $(Li_2CO_3)_8$ cluster or molten carbonate is indeed very feasible.

4. Conclusions

In conclusion, the H^+-transfer in $(CO_3)^{2-}$, Li_2CO_3 and $(Li_2CO_3)_8$ cluster were investigated by first principles calculation. On the basis of the transition state theory and calculated energetics, we found that H^+-rotation along one oxygen atom on $(CO_3)^{2-}$ was much easier than H^+-transfer between two oxygen atoms on $(CO_3)^{2-}$, indicating that a faster H^+-transfer relies upon the orientation of $(CO_3)^{2-}$. Four plausible H^+-transfer pathways in a crystalline Li_2CO_3 were also analyzed. The calculated energetics suggested that the $[001]$ and $[00\bar{1}]$ directions (C-axis) were the most favorable pathways for H^+-transfer in Li_2CO_3. The lower energy barrier was originated from the crystallographic orientation of $(CO_3)^{2-}$ perpendicular to C-axis, making H^+-rotation along O much easier. Furthermore, $(Li_2CO_3)_8$ cluster was used to simulate H^+-transfer in disordered molten carbonates. The extremely low H^+-migration energy barrier indicated that the H^+-transfer in $(Li_2CO_3)_8$ cluster and therefore molten carbonate was a very facile process. Overall, the computational results obtained clearly support the experimental observations that fast H^+-transport in molten carbonate is very feasible for dual-phase ceramic-carbonate electrolytes used in IT-SOFCs.

Acknowledgements

RSC Advances Accepted Manuscript

Financial supports from NSF (CBET-1340269, CBET-1264706), U. S. Army Research Office (W911NF-10-R-006 and W911NF-13-1-0158) are greatly appreciated.

References

1. A. Bodén, J. Di, C. Lagergren, G. Lindbergh, C. Y. Wang, *J. Power Sources*, 2007, **172**, 520–529.

2. B. Zhu, X. Liu, P. Zhou, X. Yang, Z. Zhu, W. Zhu, *Electrochem. Commun.*, 2001, **3**, 566-571.

3. B. Zhu, *J. Power Sources*, 2003, **114**, 1–9.

4. B. Zhu, X. T. Yang, J. Xu, Z. G. Zhu, S. J. Ji, M. T. Sun, J. C. Sun, *J. Power Sources*, 2003, **118**, 47–53.

5. J. Di, M. Chen, C. Wang, J. Zheng, L. Fan, B. Zhu, *J. Power Sources*, 2010, **195**, 4695–4699.

6. L. Fan, G. Zhang, M. Chen, C. Wang, J. Di, B. Zhu, *Int. J. Electrochem. Sci.,* 2012, **7**, 8420 – 8435.

7. Y. Li, Z. Rui, C. Xia, M. Anderson, Y. S. Lin, *Catal. Today*, 2009, **148**, 303–309.

8. C. Xia, Y. Li, Y. Tian, Q. Liu, Y. Zhao, L. Jia, Y. Li, *J. Power Sources*, 2009, **188**, 156–162.

9. C. Xia, Y. Li, Y. Tian, Q. Liu, Z. Wang, L. Jia, Y. Zhao, Y. Li, *J. Power Sources*, 2010, **195**, 3149–3154.

10. X. Li, N. Xu, L. Zhang, K. Huang, *Electrochem. Commun.*, 2011, **13**, 694–697.

11. François Fillaux. *J. Mol. Struct.*, 2007, **844–845**, 308–318.

12. P. D. Dopieralski, Z. Latajka and I. Olovsson. *Acta Cryst.*, 2010, **B66**, 222–228.

13. G. Kresse, J. Hafner, *Phys. Rev. B*, 1993, **47**, 558-561.

14. G. Kresse, J. Furthmüller, *Phys. Rev. B*, 1996, **54**, 11169-11186.

15. P. E. Blöchl, *Phys. Rev. B*, 1994, **50**, 17953-17979.

16. G. Kresse, D. Joubert, *Phys. Rev. B*, 1999, **59**, 1758-1775.

17. J. P. Perdew, K. Burke, M. Ernzerhof, *Phys. Rev. Lett.*, 1996, **77**, 3865–3868.

18. G. Henkelman, B. P. Uberuaga, H. Jonsson, *J. Chem. Phys.*, 2000, **113**, 9901.

19. Gaussian 09, Revision D.01, M. J. Frisch, G. W. Trucks, H. B. Schlegel, G. E. Scuseria, M. A. Robb, J. R. Cheeseman, G. Scalmani, V. Barone, B. Mennucci, G. A. Petersson, H. Nakatsuji, M. Caricato, X. Li, H. P. Hratchian, A. F. Izmaylov, J. Bloino, G. Zheng, J. L. Sonnenberg, M. Hada, M. Ehara, K. Toyota, R. Fukuda, J. Hasegawa, M. Ishida, T. Nakajima, Y. Honda, O. Kitao, H. Nakai, T. Vreven, J. A. Montgomery, Jr., J. E. Peralta, F. Ogliaro, M. Bearpark, J. J. Heyd, E. Brothers, K. N. Kudin, V. N.

RSC Advances Accepted Manuscript

Staroverov, R. Kobayashi, J. Normand, K. Raghavachari, A. Rendell, J. C. Burant, S. S. Iyengar, J. Tomasi, M. Cossi, N. Rega, J. M. Millam, M. Klene, J. E. Knox, J. B. Cross, V. Bakken, C. Adamo, J. Jaramillo, R. Gomperts, R. E. Stratmann, O. Yazyev, A. J. Austin, R. Cammi, C. Pomelli, J. W. Ochterski, R. L. Martin, K. Morokuma, V. G. Zakrzewski, G. A. Voth, P. Salvador, J. J. Dannenberg, S. Dapprich, A. D. Daniels, Ö. Farkas, J. B. Foresman, J. V. Ortiz, J. Cioslowski, and D. J. Fox, Gaussian, Inc., Wallingford CT, 2009.

20. C. Lee, W. Yang, R. G. Parr, *Phys. Rev. B*, 1988, **37**, 785–789.

21. A. D. Becke, *Phys. Rev. A*, 1988, **38**, 3098–3100.

22. A. D. McLean, G. S. Chandler, *Chem. Phys.* 1980, **72**, 5639–5648.

23. K. Raghavachari, J. S. Binkley, R. Seeger, J. A. Pople, *J. Chem. Phys.* 1980, **72**, 650–654.

24. T. Clark, J. Chandrasekhar, G. W. Spitznagel, P. V. R. Schleyer, *J. Comput. Chem.* 1983, **4**, 294–301.

25. W. R. Carper, P. G. Wahlbeck, and T. R. Griffiths, *J. Phys. Chem. B*, 2012, **116**, 5559−5567.

26. C. Y. Qin, A. Gladney, *Comput. Theor. Chem.*, 2012, **999**, 179–183.

27. M. H. Brooker and J. B. Bates, *J. Chem. Phys.* 1971, **54**, 4788.

28. A. Grzechnik, P. Bouvier, and Farina L., *J. Solid State Chem.*, 2003, **173**, 13–19.

RSC Advances Accepted Manuscript

Table 1. Energy barriers of proton migration along the pathway [100] and [$\bar{1}$00] direction.

[100]	T_{ab}	T_{bc}	R_{cd}	T_{da}
Barriers (eV)	0.85	0.78	0.58	0.90
[$\bar{1}$00]	T_{ad}	R_{dc}	T_{cb}	T_{ba}
Barriers (eV)	0.79	0.58	0.84	0.85

Table 2. Energy barriers of proton migration along the pathway [010] and [0$\bar{1}$0] direction.

[010]	T_{ef}	T_{fg}
Barriers (eV)	0.37	1.10
[0$\bar{1}$0]	T_{gf}	T_{fe}
Barriers (eV)	0.83	0.60

Table 3. Energy barriers of proton migration along the pathway [001] and [00$\bar{1}$] direction.

[001]	T_{hi}	R_{ij}	T_{jh}
Barriers (eV)	0.33	0.20	0.34
[00$\bar{1}$]	T_{hj}	R_{ji}	T_{ih}
Barriers (eV)	0.21	0.48	0.18

Table 4. Energy barriers of proton migration along the pathway [101] and [$\bar{1}$0$\bar{1}$] direction.

[101]	R_{kl}	T_{lm}	R_{mn}	T_{no}	R_{op}	T_{pk}
Barriers (eV)	1.13	0.84	0.32	0.11	0.49	0.02
[$\bar{1}$0$\bar{1}$]	T_{kp}	R_{po}	T_{on}	R_{nm}	T_{ml}	R_{lk}
Barriers (eV)	0.12	0.49	0.02	0.54	0.84	0.91

RSC Advances Accepted Manuscript

Figure Captions

Fig. 1. The optimized structures of $(CO_3)^{2-}$ and $(CO_3H)^-$ ions. The grey, red, and white balls represent the carbon, oxygen, and hydrogen atom, respectively.

Fig. 2. The energy barrier of proton transfer in the $(CO_3)^{2-}$ ionic cluster. (a) H^+-transfer between O1 and O2, (b) H^+-transfer via rotation along the O1. The grey, red, and white balls represent the carbon, oxygen, and hydrogen atom, respectively.

Fig. 3. The optimized triclinic crystal structure of Li_2CO_3; (a) primitive cell; (b) supercell structure in $1\times2\times2$ array. The purple, red, and grey balls represent the lithium, oxygen, and carbon atom, respectively.

Fig. 4. Schematic representations of H^+-transfer along (a) [100], (b) [010], (c) [001] and (d) [101] directions, respectively. The primitive cell is indicated by dashed lines.

Fig. 5. The structure of $(Li_2CO_3)_8$ cluster and the structural states of beginning, transitioning and ending phases of proton transfer in a $[(Li_2CO_3)_8H]^+$ cluster together with the relative energies. The purple, grey, red, and white balls represent the lithium, carbon, oxygen, and hydrogen atom, respectively.

RSC Advances Accepted Manuscript

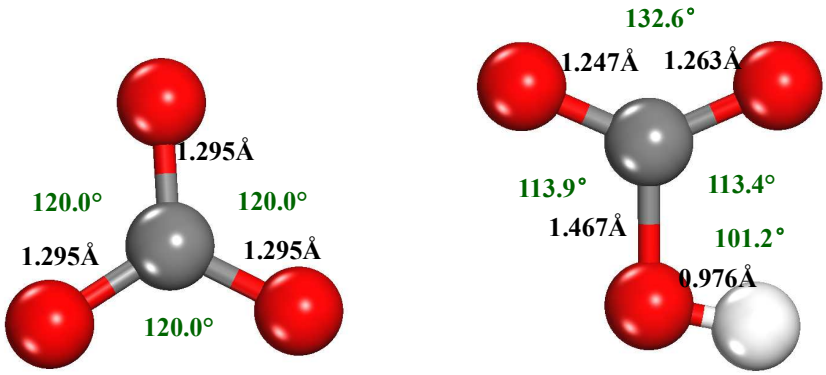

$(CO_3)^{2-}$ $(CO_3H)^{-}$

Fig. 1

RSC Advances Accepted Manuscript

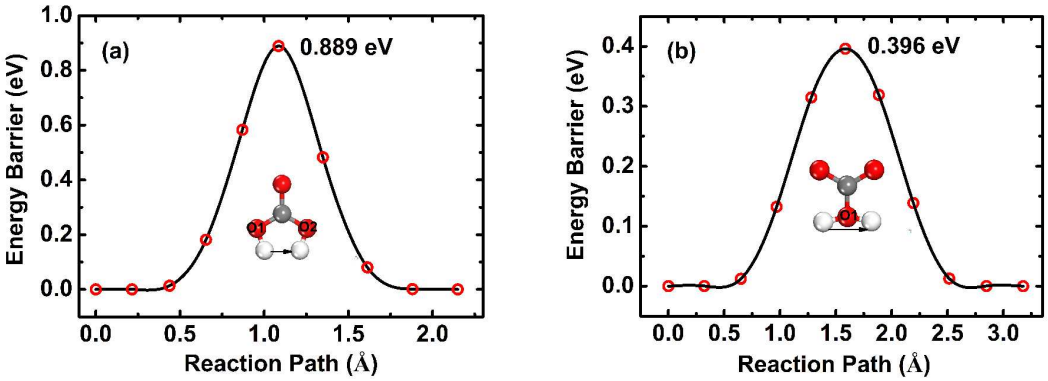

Fig. 2

RSC Advances Accepted Manuscript

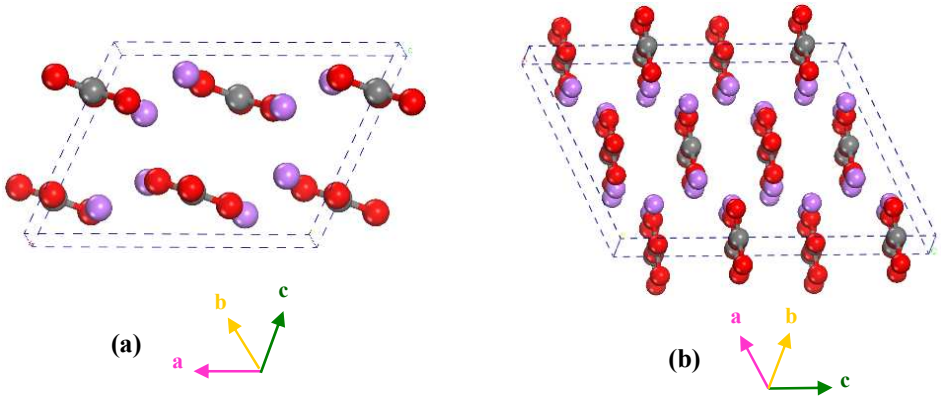

Fig. 3

RSC Advances Accepted Manuscript

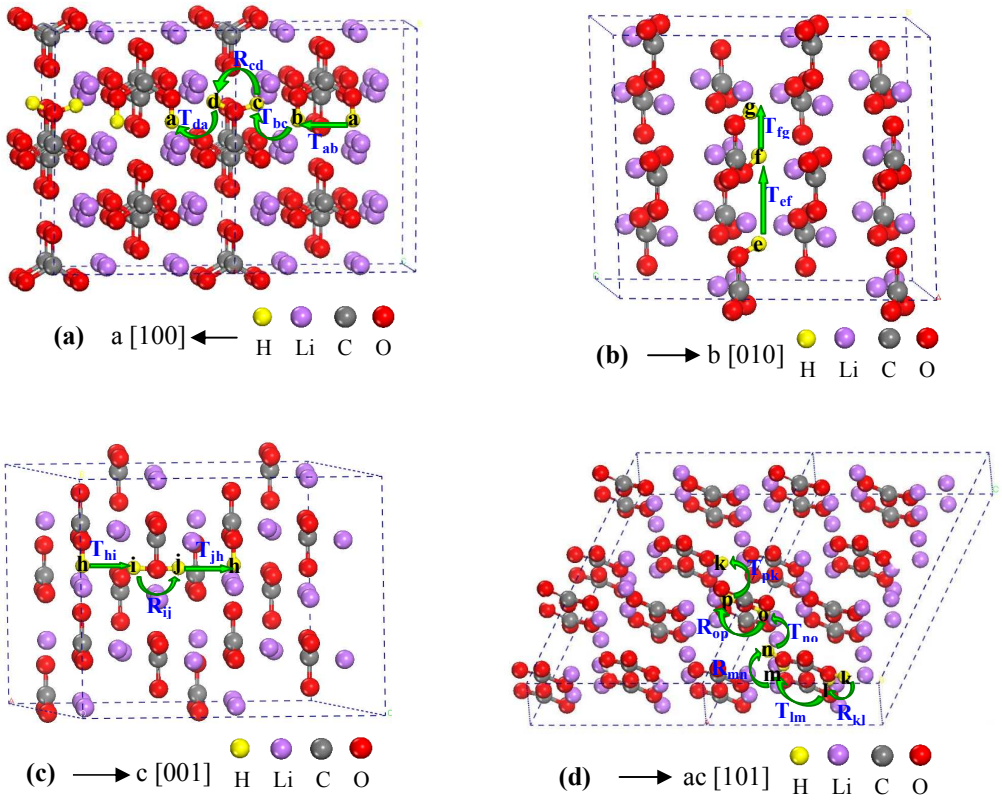

Fig. 4

RSC Advances Accepted Manuscript

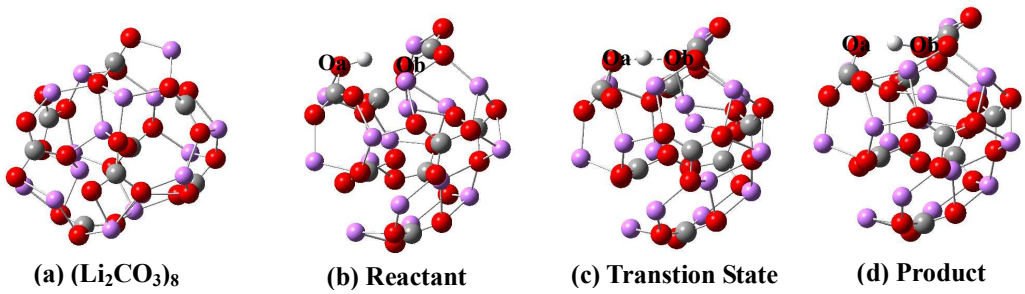

(a) $(Li_2CO_3)_8$ (b) Reactant (c) Transtion State (d) Product

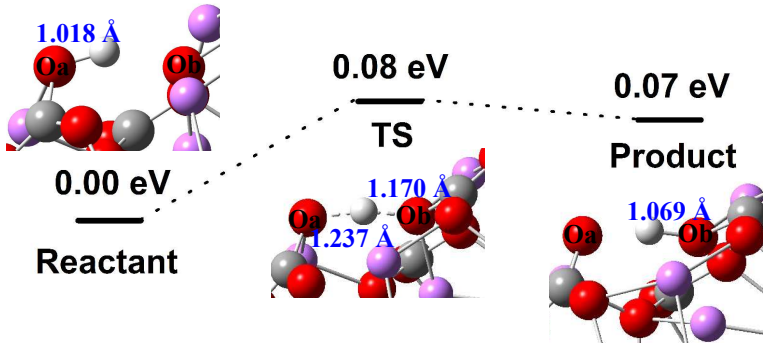

Fig. 5

RSC Advances Accepted Manuscript